

Study of Frictional and Impact Transients in Active-Passive Mechanical Pair

Michael Ruderman and Francesco De Rito

Abstract—We consider an active-passive mechanical pair in which the relative motion of the latter is constrained by the mechanical impact. The system dynamics is described by the previously introduced modeling frameworks of force transition and dissipation through the nonlinear Coulomb friction and structural damping, the later in accord with Hertzian contact theory. The focus of the recent study is on combining both interaction mechanisms, and the detailed experimental evaluation which discloses validity of the modeling assumptions. Such mechanical pair interactions can be found in various mechatronic systems and mechanisms, like for example clutches, backlash elements, sliding items on the shaking and inclining surfaces, conveyor belts and others. This practical study demonstrates and discusses the transients of a vibro-impact dynamics and shows theoretical developments in line with experimental evaluation.

I. INTRODUCTION

Multiple mechatronic systems and mechanisms involve nonsmooth dynamics (see e.g. [1] for basics) with impacts, in addition to kinetic friction (see e.g. [2] for introduction) of the moving parts in contact with each other. Both well-known mechanical effects are often unavoidable due to the structural properties and the corresponding functionality of a mechanism at hand. Both also involve the associated energy dissipation (mostly nonlinear in the nature) and influence (in more peculiar way) the transient behavior of each mechanical pair. One of the clearest examples of the combined effect of impact and friction dynamics is backlash [3], also known as mechanical play. Hybrid approaches are known for modeling and controlling backlash, e.g. [4], and detecting and identifying it [5], [6]. Apart from the backlash, the vibro-impact applications can be found, for instance, in clutches, forging and riveting machines, pneumatic and hydraulic hammers and drills (cf. e.g. [7] for basics), but also in shaking and tilting surfaces, conveyor belts and more. Later, the impact dynamics with restitution [8] was found useful even in the robotics, for simulating contacts with environment e.g. [9], or by attempting to describe the walking gait of walking robots, cf. e.g. [10].

Systems which include nonsmooth mechanics are understood to have hybrid dynamics [11], with the corresponding guard and jump maps in the state space, and (eventually) differential inclusions instead of differential equations where necessary. Such systems become hybrid in terms of continuous

and switched solutions (correspondingly state trajectories) and require particular attention in every respect when it comes to modeling, identification, and control. For a tutorial on nonsmooth analysis and stability we refer to e.g. [12]. For basics on hybrid and switched systems, see also [13].

In this paper, two modeling approaches are combined together for describing and experimentally studying the frictional and impact transients in an active-passive mechanical pair. The first modeling framework, introduced in [14], formalizes the dynamic interactions of two inertial bodies that are connected to each other exclusively via the friction surface and governed by the nonlinear Coulomb friction. The second modeling approach [15] originates from describing the contact force and corresponding structural damping of the impact in a backlash pair, while using the restitution and damping laws formulated in [8]. Dynamic equations of both modelings are combined in a hybrid setting, and share the same state variables and switching conditions. One of the cores of this study is a series of experiments designed for the dedicated laboratory setup to reveal meaningful motion transitions.

The rest of the paper is organized as follows. In section II, we provide the necessary preliminaries of the overall system modeling, following the original works [14], [15]. Section III describes the used tribological setup, cf. [16], specially developed for frictional and impact experiments with one active and one passive moving body in contact. The comparison between the modeled and measured system response is reported in section IV. The paper is briefly concluded by section V.

II. PRELIMINARIES

In this section, we first recall both modeling frameworks [15] and [14] used for describing the frictional and impact transients in an active-passive mechanical pair. A principal structure of an active-passive mechanical pair is shown in Fig. 1, with the corresponding action and reaction flow.

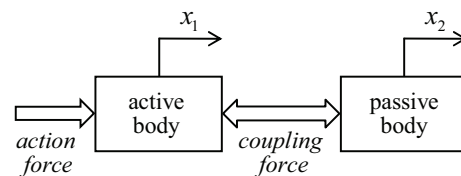


Fig. 1: Action and reaction flow in active-passive pair.

A. Coupling via frictional interface

Considering a mechanical pair consisting of an active and a passive subsystem, the relative motion of the first occurs in

arXiv:2501.03653v1 [eess.SY] 7 Jan 2025

M. Ruderman is with Department of Engineering Sciences, University of Agder (UiA). Postal address: P.B. 422, Kristiansand, 4604, Norway.

Corresponding author: email michael.ruderman@uia.no

F. De Rito is with University of Padova, Vicenza, Italy.

This work was partially supported by the ERASMUS+ program.

the coordinates x_1 and that of the second in x_2 , cf. Fig. 1. Both are in the generalized coordinates (either translational or rotational) with one degree of freedom and governed by

$$\ddot{x}_1(t) = f_1(x_1(t), x_2(t), t), \quad \ddot{x}_2(t) = f_2(x_2(t), x_1(t)). \quad (1)$$

Note that the second subsystem in (1) is semi-autonomous and depends explicitly on the dynamic trajectories of the first one.

$$x_1 - x_2 =: z, \quad (2)$$

$$\left(m_1 + m_2(1 - |\operatorname{sgn}(\dot{z})|)\right) \ddot{x}_1 + a_1 \dot{x}_1 + a_2 x_1 + b \operatorname{sgn}(\dot{z}) = u, \quad (3)$$

$$m_2 \ddot{x}_1 \left(1 - |\operatorname{sgn}(\dot{z})|\right) \frac{1}{2} \left(1 - \operatorname{sgn}(|\dot{x}_1| - b m_2^{-1})\right) - m_2 \ddot{x}_2 + b \operatorname{sgn}(\dot{z}) = 0. \quad (4)$$

Here the dynamics equations (2)–(4) correspond to the system (1) for the case where the first active body with the mass m_1 is feedback controlled, while the coefficients $a_1, a_2 > 0$ accommodate both the state feedback gains and (eventually) structural properties of the active subsystem, like e.g. restoring spring and viscous damping. Note that the state variables and signals in (2)–(4) are without time argument for the sake of brevity. The exogenous value $u(t)$ can be seen here as, for example, a reference trajectory generator for the feedback-controlled active subsystem (3). The coupling between both subsystems occurs essentially due to the nonlinear Coulomb friction with the coefficient $b > 0$. When the passive body slips over the active one, the relative velocity between the both is $\dot{z} \neq 0$. Otherwise, both subsystems are considered to be in a coupled state with $\dot{z} = 0$, that affects correspondingly the dynamics (3), (4). Important to notice is also that the classical three-point-valued signum function is used here, i.e.

$$\operatorname{sgn}(y) = \begin{cases} 1, & y > 0, \\ 0, & y = 0, \\ -1, & y < 0, \end{cases} \quad (5)$$

where an argument y is the real number.

Further, it must be noted that if the active subsystem is robustly controlled, i.e. the contact frictional force $b \operatorname{sgn}(\dot{z})$ is not propagated back so as to affect the motion trajectories $(x_1(t), \dot{x}_1(t))$, then the equation (3) is substituted by

$$\ddot{x}_1(t) = f_1(t). \quad (6)$$

This is particularly the case we are going to consider in the current study. For more details on the hybrid dynamics (2)–(4), an interested reader is further referred to [14].

B. Vibro-impact dynamics

Upon contacting with mechanical motion limiters, the moving body m_2 experiences impact transitions, which are associated with a resulting repulsion force and structural damping. In case of repetitive impact and separation, the so-called vibro-impact system emerges, while the colliding body m_2 can be assumed as absolutely stiff and the fixed frame as elastic, this

Assuming a flat and unconstrained contact of both mechanical bodies of the subsystems given in (1), which is due to a normal load provided by the lumped mass m_2 , the generic modeling framework of the corresponding frictional coupling was introduced in [14]. The transient and steady-state behavior of the both moving bodies is captured by

for the sake of simplicity and without loss of generality. Note that this assumption is also in line with the general Hertzian theory of non-adhesive elastic contacts.

The vibro-impact dynamics assumes $\dot{x}_2^o = -e \dot{x}_2^i$, where the relative displacement rates are denoted by the superscripts $\{i, o\}$, for indicating before (“in”) and, correspondingly, after (“out”) the collision. Here we recall that the restitution coefficient $e \in [0, 1]$ reduces the relative velocity and, usually, is interpreted as a measure of the degree of energy dissipation during an impact. Also we note that the lower and upper boundaries of e represent an absolute plastic and, respectively, absolute elastic contact. For a limited range of relatively low velocities, and for the most of materials with a linear elastic range, it can be written with a tolerable accuracy [8]:

$$e = 1 - \alpha \dot{x}_2^i.$$

The coefficient α is characteristic for each considered elastic material and geometry of the structure. During a vibro-impact transition, the overall contact force is also including the nonlinear structural damping, following [8]. Capturing the state of penetration of the body m_2 into the elastic frame by

$$p(t) = \int_{t^i}^{t^o} \dot{x}_2(t) dt,$$

where the integration limits t^i and t^o indicate the time instants of the impact and separation, respectively, the contact force is modeled as in [15] by

$$f(p) = \lambda p^n \dot{p} + k p^n. \quad (7)$$

The coefficient $\lambda = 1.5\alpha k$ is based on the energetic balance of the restitution derived in [8]. For the construction materials (like e.g. steel or aluminium) α has a relatively small value, thus keeping impact in a predominantly elastic region. However, one can recognize a multiplicative coupling between α and k , so that a practical identification will have a trade-off between the used experimental data and interpretation of the values range of the determined parameters. The contact

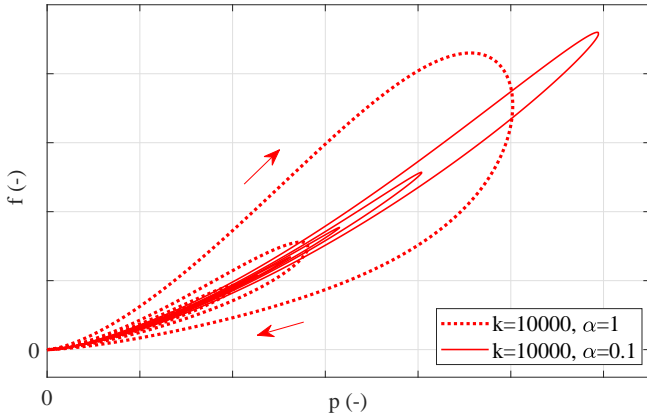


Fig. 2: Exemplary (p, f) map for different α parameters.

stiffness coefficient is $k > 0$, and the structural damping increases with the depth of penetration, i.e. with $\dot{p} > 0$. It is also worth recalling that for $n = 3/2$, the vibro-impact dynamics is consistent with the Herzian theory of contacting spheres under static conditions, while for $n = 1$ it captures the most simple case of two flat surfaces, cf. [8].

One of the important features of the vibro-impact dynamics (7) is that the contact force is zero at the instants of impact and separation, the feature which cannot be provided by the modeling approaches which incorporate a linear damping $\sigma \dot{x}_2$. Worth noting is also that this is independent of the velocity magnitude $|\dot{x}_2^i| < \Omega$ at the moment of contact, while the validity range is limited by some finite $0 < \Omega < \infty$, cf. [8]. An illustrative example of how the contact force (7) develops for a series of $p(t)$ cycles with a decreasing amplitude is shown in Fig. 2. Here, the arbitrarily assumed stiffness coefficient $k = 10000$ is kept the same, while the compared $\alpha = \{0.1, 1\}$ factors are differing by the order of magnitude. One can recognize the shaping effect of α , that gives rise also to a larger area of the vibro-impact hysteresis loop and, thus, structural dissipation at each closed cycle of penetration.

III. EXPERIMENTAL SETUP

A tribological experimental setup used in this study is shown (laboratory view) in Fig. 3, see [16] for details. The linear moving platform, which is an active subsystem, is arranged under and aligned with the fixed mechanical frame. The lumped disk, which is a passive subsystem m_2 , is guided within the mechanical frame. Note that the lateral contacts between the disc and the walls of the frame-slot are minimized by the specially machined side-edging on the disc. This way the side-contact friction with the walls can be neglected, and the single essential frictional interface is associated the disc staying horizontally on the moving platform. Two disk samples are used: one from the steel with the mass $m_2' = 0.052$ kg, and one from the aluminium with the mass $m_2'' = 0.024$ kg. The corresponding Coulomb friction coefficients are $b' = \mu' m_2' g = 0.214$ N and $b'' = \mu'' m_2'' g = 0.1106$ N, where g is the gravitational acceleration constant and μ' , μ'' are the



Fig. 3: Experimental setup of controlled active subsystem with passive mass put on the flat surface of the moving platform.

nominal friction coefficients. The latter are assumed as the known standard values for the steel-on-steel and aluminium-on-steel pairs, respectively. The moving platform is actuated by a servo-drive with the stiff high-precision ball-screw, so that the feedback controlled linear displacement $x_1(t)$ can be directly commanded. The constant steady-state velocity, used in one of the following experiments, is $\dot{x}_1(t) = 0.1$ m/sec. This is the maximal possible value provided by specification of the BLDC-motor driven ball-screw stage. The absolute position of the passive disk $x_2(t)$ is measured by a high-resolution laser sensor with the nominal repeatability of $8 \mu\text{m}$. The sampling rate of the data acquisition real-time board is set to 5 kHz.

IV. COMPARISON OF THE MODELED AND MEASURED RESPONSE

Both modeling frameworks, summarized in sections II-A and II-B, are combined to represent the dynamic behavior of the passive body m_2 experiencing an elastic contact with the fixed frame under the condition $\dot{x}_1 = \text{const}$. This leads to reduction of (2)–(4) and, after incorporating (7), results in the overall hybrid system dynamics

$$x_1 - x_2 =: z, \quad (8)$$

$$\dot{x}_1 = \text{const}, \quad (9)$$

$$\frac{1}{2} \left(1 + \text{sgn}(x_2 - X_c) \right) (x_2 - X_c) =: p, \quad (10)$$

$$m_2 \ddot{x}_2 - b \text{sgn}(\dot{z}) + f(p, t) = 0. \quad (11)$$

The threshold value $X_c = \text{const}$ represents the position of the impact. Following to that, the internal (virtual) state $p(t)$ constitutes the penetration of the impacting body m_2 into an elastic structure of the fixed frame, cf. Fig. 4.

Two different experimental scenarios were conducted and compared with the modeled behavior. Both are designed to be conclusive and complementary to each other in evaluation of the modeling framework (8)–(11).

In the first one, the active mechanical subsystem was in the idle state, implying $\dot{x}_1 = \text{const} = 0$, and an impulsive excitation was provided to the passive body via a rubber hammer, that is often used in the structural modal analysis. For this type

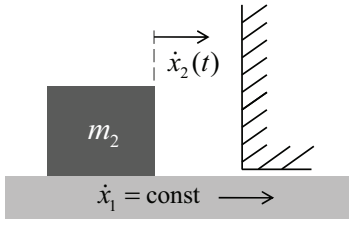


Fig. 4: Schematic representation of the active-passive pair.

of experiments, the steel disk was taken since it discloses a more stable translational motion during and after the impact with the fixed frame, i.e. no tilting-type separation of the horizontal contact from the supporting platform (i.e. active subsystem m_1). The enforced excitation provided a sufficiently high relative velocity of the free moving body m_2 , and allowed for the values $\dot{x}_2^+ \approx 1$ m/sec before the collision. The measured and model fitted vibro-impact response is exemplary shown in Fig. 5. Note that the experimental relative velocity \dot{x}_2 is obtained by the discrete time differentiation of the measured position $x_2(t)$ with a subsequent low-pass filtering.

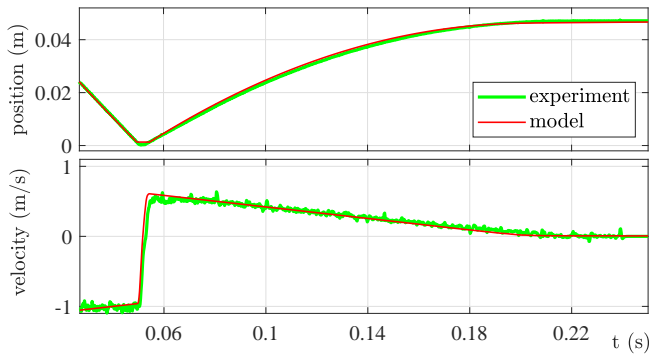


Fig. 5: Measured and model fitted vibro-impact response.

The second experimental scenario was designed for the maximal possible constant velocity of the active subsystem $\dot{x}_1 = 0.1$ m/sec while the passive body m_2 came to contact with the frame and, afterwards, experienced a series of vibro-impact transitions. The latter occurred due to an interplay of the repulsive contact force, Coulomb friction damping, and a continuous motion of the active part of the contact pair, i.e. $\dot{x}_1 = \text{const} \neq 0$, cf. (8)–(11). Here the aluminium disk was used due to its lower mass and friction coefficient μ'' , that leads in a larger repulsive displacement and, thus, higher number of the vibro-impact cycles. The measured and model-fitted vibro-impact response are exemplary shown in Fig. 6. Note that $t = 0$ and $x_2(0)$ are shifted here for the sake of a better visualization, while X_c parameter is highly sensitive due to the process noise and uncertain touching point of the laser beam to the moving disc m_2 , cf. Fig. 3.

V. CONCLUSIONS

In this paper, an experimental case study was developed, performed on a dedicated tribological setup, [16], while com-

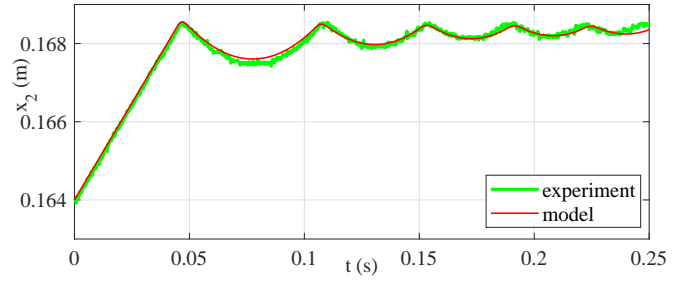


Fig. 6: Measured and model fitted vibro-impact response.

binning the Coulomb based friction coupling [14] with the nonlinear structural damping modeling [15] based on [8]. The overall hybrid dynamics framework was formulated for the given mechanical structure, and two specific experimental scenarios were designed and performed for collecting the motion data of a passive inertial body. This one was subject to elastic vibro-impact with a fixed frame and normal frictional interface to an active body – the moving and supporting platform. It was shown how the nonlinear mechanisms of the Coulomb friction coupling and the contact restitution are superimposed and able to adequately capture the transient system behavior. The demonstrated accord between the measured and model-predicted displacement response supported this.

REFERENCES

- [1] B. Brogliato, *Nonsmooth Mechanics: Models, Dynamics and Control*, 3rd ed. Springer, 2016.
- [2] M. Ruderman, *Analysis and compensation of kinetic friction in robotic and mechatronic control systems*. CRC Press, 2023.
- [3] T. Goodman, “Dynamic effects of backlash,” *Machine Design*, vol. 35, no. 12, pp. 150–157, 1963.
- [4] P. Rostalski, T. Besselmann, M. Baric, F. Van Belzen, and M. Morari, “A hybrid approach to modelling, control and state estimation of mechanical systems with backlash,” *International Journal of Control*, vol. 80, no. 11, pp. 1729–1740, 2007.
- [5] M. Ruderman, S. Yamada, and H. Fujimoto, “Backlash identification in two-mass systems by delayed relay feedback,” *Journal of Dynamic Systems, Measurement, and Control*, vol. 141, no. 6, p. 061007, 2019.
- [6] M. Ruderman and L. Fridman, “Model-free sliding-mode-based detection and estimation of backlash in drives with single encoder,” *IEEE Trans. on Control Systems Technology*, vol. 29, pp. 812–817, 2021.
- [7] V. Babitsky, *Theory of vibro-impact systems & applic.* Springer, 1998.
- [8] K. Hunt and F. Crossley, “Coefficient of restitution interpreted as damping in vibroimpact,” *Journal of Applied Mechanics*, vol. 42, 1975.
- [9] D. W. Marhefka and D. E. Orin, “Simulation of contact using a nonlinear damping model,” in *IEEE International Conference on Robotics and Automation (ICRA)*, vol. 2, 1996, pp. 1662–1668.
- [10] L. Freidovich, U. Mettin, A. Shiriaev, and M. Spong, “A passive 2-DOF walker: Hunting for gaits using virtual holonomic constraints,” *IEEE Transactions on Robotics*, vol. 25, no. 5, pp. 1202–1208, 2009.
- [11] R. Goebel, R. Sanfelice, and A. R. Teel, “Hybrid dynamical systems,” *IEEE Control Systems Magazine*, vol. 29, no. 2, pp. 28–93, 2009.
- [12] J. Cortes, “Discontinuous dynamical systems,” *IEEE Control Systems Magazine*, vol. 28, no. 3, pp. 36–73, 2008.
- [13] D. Liberzon, *Switching in systems and control*. Springer, 2003.
- [14] M. Ruderman, A. Zagvozdkin, and D. Rachinskii, “Dynamics of inertial pair coupled via frictional interface,” in *IEEE 61st Conference on Decision and Control (CDC)*, 2022, pp. 1324–1329.
- [15] M. Ruderman, “On stiffness and damping of vibro-impact dynamics of backlash,” in *IEEE 30th International Symposium on Industrial Electronics (ISIE)*, 2021, pp. 1–4.
- [16] M. Ruderman, “Robust asymptotic observer of motion states with nonlinear friction,” *IFAC-PapersOnLine*, vol. 56, pp. 5931–5936, 2023.